Biophysical Journal Volume 73 September 1997 1410–1423

A Generalized Activating Function for Predicting Virtual Electrodes in Cardiac Tissue

Eric A. Sobie, Robert C. Susil, and Leslie Tung
The Johns Hopkins University School of Medicine, Department of Biomedical Engineering, Baltimore, Maryland 21205 USA

ABSTRACT To fully understand the mechanisms of defibrillation, it is critical to know how a given electrical stimulus causes membrane polarizations in cardiac tissue. We have extended the concept of the activating function, originally used to describe neuronal stimulation, to derive a new expression that identifies the sources that drive changes in transmembrane potential. Source terms, or virtual electrodes, consist of either second derivatives of extracellular potential weighted by intracellular conductivity or extracellular potential gradients weighted by derivatives of intracellular conductivity. The full response of passive tissue can be considered, in simple cases, to be a convolution of this "generalized activating function" with the impulse response of the tissue. Computer simulations of a two-dimensional sheet of passive myocardium under steady-state conditions demonstrate that this source term is useful for estimating the effects of applied electrical stimuli. The generalized activating function predicts oppositely polarized regions of tissue when unequally anisotropic tissue is point stimulated and a monopolar response when a point stimulus is applied to isotropic tissue. In the bulk of the myocardium, this new expression is helpful for understanding mechanisms by which virtual electrodes can be produced, such as the hypothetical "sawtooth" pattern of polarization, as well as polarization owing to regions of depressed conductivity, missing cells or clefts, changes in fiber diameter, or fiber curvature. In comparing solutions obtained with an assumed extracellular potential distribution to those with fully coupled intra- and extracellular domains, we find that the former provides a reliable estimate of the total solution. Thus the generalized activating function that we have derived provides a useful way of understanding virtual electrode effects in cardiac tissue.

INTRODUCTION

The question of how an applied electric field affects the heart is of fundamental importance in cardiac electrophysiology, particularly as it relates to widespread clinical treatment of defibrillation. The mechanisms of defibrillation, while largely unresolved, are known to involve changes in the transmembrane potentials of cardiac cells (Witkowski and Kerber, 1991; Walcott et al., 1994). Thus the effects a given electrical stimulus will have on the transmembrane potential in a region of tissue (i.e., whether it depolarizes or hyperpolarizes the membrane, and the magnitude of this polarization) are very relevant.

Theoretical models and computer simulations have proved to be valuable in understanding the mechanisms of electrical stimulation of cardiac tissue (and of other excitable tissues as well). Obviously, theorizing alone cannot replace rigorous and well-designed experiments, but the proper framework for considering the problem of electrical stimulation can help in making predictions and gaining insight from previously obtained results. The body of theoretical and computational work that relates to cardiac stimulation is considerable, and many possible mechanisms for stimulation have been described (for review see Roth, 1994, Roth and Wikswo, 1996). These mechanisms can be divided into effects that occur close to the stimulating electrodes or tissue boundaries, so-called near-field or boundary effects, and those that occur far away from the electrodes, in the bulk of the myocardium, which we will refer to as bulk effects. Examples of the former include the fall-off in potential due to current redistribution near a tissue border, and the "dog bone" pattern of membrane polarization and virtual electrode effects caused by point stimulation of tissue (Sepulveda et al., 1989; Knisley et al., 1994). Most investigations to date on possible bulk mechanisms have focused on the predicted "sawtooth" potential pattern produced by relatively high resistance gap junctions between adjacent cells (Plonsey and Barr, 1986a; Krassowska et al., 1987; Cartee and Plonsey, 1992; Trayanova and Pilkington, 1993), but recently it has been suggested that fiber curvature and fiber branching may also contribute to membrane polarization away from the electrodes (Trayanova and Roth, 1992; Trayanova et al., 1993). With few recent exceptions (Trayanova, 1996), the analyses of boundary and bulk effects have tended to proceed along different lines, and the two cases have been considered to occur by different mechanisms. To date, little has been done to develop a common framework for understanding different mechanisms of cardiac stimulation.

Rattay, in analyzing the stimulation of a neuron by a point source, used the phrase "activating function" to describe the source term that acted to excite the fiber (Rattay, 1986, 1988). Building on the earlier work of McNeal (1976), Rattay noted that the second derivative of extracellular potential along the fiber axis drove changes in transmem-

Received for publication 11 November 1996 and in final form 23 April 1997.

Address reprint requests to Dr. Leslie Tung, The Johns Hopkins University School of Medicine, 720 Rutland Avenue, 703 Traylor Building, Baltimore, MD 21205. Tel.: 410-955-7453; Fax: 410-955-0549; E-mail: ltung@bme.jhu.edu.

0006-3495/97/09/1410/14 $2.00

brane potential. Since these investigations several other researchers have examined and applied these ideas to their studies of electrical stimulation (Warman et al., 1992; Plonsey and Barr, 1995; Neunlist and Tung, 1995). It is now widely recognized that although the activating function does not describe the full response of the fiber, it can be useful for predicting the locations and magnitudes of the current sources that will influence the membrane, for determining the initial change in transmembrane potential at all points along the fiber, and for estimating the eventual pattern of transmembrane potentials in the nerve fiber (Altman and Plonsey, 1990; Roth, 1994; Durand, 1995). However, because a neuron is thin enough that it can be considered isopotential across its diameter, this analysis has been confined to the one-dimensional case and has not been widely used to study cardiac stimulation, where the anisotropy inherent in cardiac tissue (Clerc, 1976; Roberts et al., 1979) can play an important role in stimulation. The application of these concepts has also been limited because the activating function implicitly assumes that the potentials outside the tissue can be determined, are unchanging throughout the stimulus, and are affected little by the tissue transmembrane currents. In cardiac tissue, where the intracellular and extracellular domains are electrically coupled, it is not known how well these assumptions will hold when strong stimuli are applied. Thus, until now it has not been clear how applicable the idea of the activating function may be to the problem of stimulation of the heart.

In this study we demonstrate that the concept of the activating function can be extended to higher dimensions. We derive a general form for the activating function that includes contributions of nonuniform fields and nonuniform intracellular conductivities. We investigate the assumptions inherent in this formulation, and show that this "generalized activating function" is useful for understanding known mechanisms of stimulation and for predicting new ways in which virtual electrode effects can be produced. As has been shown in one-dimensional simulations (Warman et al., 1992; Neunlist and Tung, 1995; Plonsey and Barr, 1995), the response of the tissue can be thought of as a convolution of the activating function with the point response of the tissue, so the transmembrane potential distribution appears as a filtered version of the activating function.

THEORY

Derivation of the generalized activating function

Our analysis begins with the bidomain equations, which describe the relationship between potential, conductivity, and membrane current in multidimensional cardiac tissue. In regions devoid of external stimulation, the appropriate equations are (Henriquez, 1993)

$$\nabla \cdot (\mathbf{G}_i \nabla \Phi_i) = I_m \tag{1}$$

$$\nabla \cdot (\mathbf{G}_e \nabla \Phi_e) = -I_m \tag{2}$$

where Φ_i and Φ_e are the intracellular and extracellular potentials, I_m is the transmembrane current, and $\mathbf{G}_i$ and $\mathbf{G}_e$ are tensors that describe the macroscopic intracellular and extracellular conductivities, respectively. Membrane current will consist of ionic and capacitive components, so

$$I_m = I_{ion} + C_m^v \frac{\partial V_m}{\partial t} \tag{3}$$

where I_{ion} is the transmembrane ionic current, V_m is the transmembrane potential, and C_m^v is the membrane capacitance. Here, C_m^v, I_m, and I_{ion} are expressed in per-unit-volume units and are related to the corresponding area-specific variables by the tissue surface area-to-volume ratio β. In Eq. 3, we ignore the membrane potential of the resting tissue, so V_m refers to deviations from this value. Combining Eqs. 1 and 3, and using the identity $\Phi_i = V_m + \Phi_e$ yields

$$I_{ion} + C_m^v \frac{\partial V_m}{\partial t} - \nabla \cdot (\mathbf{G}_i \nabla V_m) = \nabla \cdot (\mathbf{G}_i \nabla \Phi_e) \tag{4}$$

The right-hand side is the activating function in its most general form (which we will refer to as S). When a stimulus is applied at diastole, initially V_m is zero everywhere in the tissue, and ionic current is zero, so the first and third terms on the left-hand side will drop out. Under these conditions, we see that the activating function will drive the initial change in membrane potential.

Exact and approximate steady-state solutions

Clearly, the generalized activating function represents a source term for V_m, but thus far we have said nothing about how the extracellular potential distribution is established. The circumstances of the stimulation, such as the electrode placement and the magnitude of the stimulating current, will have a large influence on the potentials and fields that exist outside the cells, and often a good prediction of these potentials can be arrived at by considering these conditions. For example, in some cases circumstances suggest that a region of tissue will experience a uniform field. We refer to this estimate as the primary potential distribution, and denote it by Φ_e^p. However, tissue membrane currents, which in general cannot be predicted a priori, will have a secondary effect on Φ_e, which can be seen by examining Eq. 2. Thus we can write the extracellular potential as the sum of the primary potential distribution, Φ_e^p, and a secondary potential, Φ_e^s, that reflects the influence of the tissue on these potentials. In other words, $\Phi_e = \Phi_e^p + \Phi_e^s$, where Φ_e represents the total, exact solution for extracellular potential that is determined by solving Eqs. 4 and 2 simultaneously. Since the extracellular potential gradient is part of the generalized activating function, we can also write this term as the sum of primary and secondary components. For passive, steady-state conditions, Eq. 4 becomes

$$\frac{V_m}{R_m^v} - \nabla \cdot (\mathbf{G}_i \nabla V_m) = \nabla \cdot (\mathbf{G}_i \nabla \Phi_e^p) + \nabla \cdot (\mathbf{G}_i \nabla \Phi_e^s) \tag{5}$$

where the volume-specific membrane resistance, R_m^v (in $\Omega \cdot cm^3$), is related to the area-specific resistance by β. An exact solution for membrane potential must take into account both components of the extracellular fields, but an approximate solution can be obtained if only the primary sources are considered, provided that the primary source term dominates the secondary source term. We expect that this will be the case in many situations, because the applied fields, and hence extracellular currents, can be large compared with the membrane currents. In some of our simulations, we will examine the validity of this assumption as well as investigate how a reliable estimate of the primary potential distribution can be obtained.

Definition of conductivity tensor

Orthotropic anisotropy is the most general case of anisotropy, and to characterize a domain of this sort we must define conductivities in each of three principal directions (Nielsen et al., 1991; Hunter et al., 1992). In light of the fibrous structure of the heart, we denote these conductivities as g_l, along the fiber axis, and g_t and g_u, in the two principal directions perpendicular to the fiber axis. In the fiber coordinate system, the conductivity tensor is diagonal:

$$\mathbf{G}_f = \begin{bmatrix} g_l & 0 & 0 \\ 0 & g_t & 0 \\ 0 & 0 & g_u \end{bmatrix} \tag{6}$$

These conductivities represent averaged values that depend on the resistivities of the domain fluids and microscopic structure of the tissue (Neu and Krassowska, 1993). Let us further define the unit vectors of the localized rectangular Cartesian axes of the cardiac fiber to be $(\hat{\mathbf{l}}, \hat{\mathbf{t}}, \hat{\mathbf{u}})$ and those of the global tissue axes to be $(\hat{\mathbf{x}}, \hat{\mathbf{y}}, \hat{\mathbf{z}})$. In general, the fiber conductivity tensor $\mathbf{G}_f$ can be transformed into the tissue coordinate system by the rotation tensor $\mathbf{A}$. If $\mathbf{G}$ is the conductivity tensor in the global coordinate system, then

$$\mathbf{G} = \begin{bmatrix} g_x & g_{xy} & g_{xz} \\ g_{xy} & g_y & g_{yz} \\ g_{xz} & g_{yz} & g_z \end{bmatrix} = \mathbf{A}\mathbf{G}_f\mathbf{A}^T \tag{7}$$

where

$$\mathbf{A} = \begin{bmatrix} l_x & t_z & u_x \\ l_y & t_y & u_y \\ l_z & t_z & u_z \end{bmatrix} \tag{8}$$

The columns of $\mathbf{A}$ are equal to the unit vectors of $(\hat{\mathbf{l}}, \hat{\mathbf{t}}, \hat{\mathbf{u}})$ expressed in tissue coordinates, i.e., where

$$\hat{\mathbf{l}} = l_x\hat{\mathbf{x}} + l_y\hat{\mathbf{y}} + l_z\hat{\mathbf{z}} \tag{9a,b,c}$$

$$\hat{\mathbf{t}} = t_x\hat{\mathbf{x}} + t_y\hat{\mathbf{y}} + t_z\hat{\mathbf{z}}$$

$$\hat{\mathbf{u}} = u_x\hat{\mathbf{x}} + u_y\hat{\mathbf{y}} + u_z\hat{\mathbf{z}}$$

In the general case, the elements of $\mathbf{A}$ can be functions of position.

Approximate time-dependent solution by convolution integral

If we are interested in solving the approximate problem for passive tissue, then the equation governing the response is

$$\frac{V_m}{R_m^v} + C_m^v \frac{\partial V_m}{\partial t} - \nabla \cdot (\mathbf{G}_i \nabla V_m) \approx \nabla \cdot (\mathbf{G}_i \nabla \Phi_e^p) \tag{10}$$

This is a linear partial differential equation for V_m, with the right-hand side acting as a source term. Because we assume that the source is unchanging throughout the stimulus, the transmembrane potential at any time during the stimulus can be solved for by standard techniques. Specifically, if we can determine the response of the tissue to an intracellular current source located anywhere in the tissue, then by superposition we can determine the total response by summing these impulse responses weighted by the magnitudes of the current at each point. These weights are given by the generalized activating function. Expressed mathematically, if $h(x, y, z, \eta, \xi, \nu, t)$ is the response at location (x, y, z) and time t to a current source located at (η, ξ, ν), and $S(x, y, z)$ describes the sources everywhere in the tissue, then the transmembrane potential at any location (x, y, z) is given by

$$V_m(x, y, z, t) = \int_{-\infty}^{\infty}\int_{-\infty}^{\infty}\int_{-\infty}^{\infty} S(\eta, \xi, \upsilon)h(x, y, z, \eta, \xi, \upsilon, t)d\eta\, d\xi\, d\upsilon \tag{11}$$

This calculation is simplified considerably if the impulse response at any point is a shifted copy of the response of a current injected anywhere else in the tissue—in other words, if the tissue is shift-invariant. This would be the case, for example, in tissue with constant fiber direction. Under these conditions the response to any source term is simply a convolution of the tissue impulse response (transfer function) $h(x, y, z, t)$ with the generalized activating function $S(x, y, z)$, or

$$V_m(x, y, z, t) = \int_{-\infty}^{\infty}\int_{-\infty}^{\infty}\int_{-\infty}^{\infty} S(\eta, \xi, \upsilon)h(x - \eta, y - \xi, z - \upsilon, t)d\eta\, d\xi\, d\upsilon \tag{12}$$

This use of a convolution integral to compute the tissue response is an extension to higher dimensions of the approach that others have used (Warman et al., 1992; Neunlist and Tung, 1995; Plonsey and Barr, 1995). Not all situations of interest are amenable to this approach, however, as the cases that will be considered will demonstrate.

Examination of the activating function

We will now examine the generalized activating function in more detail to gain an understanding of the terms that

contribute to it. If we expand the term $\nabla \cdot (\mathbf{G}_i \nabla \Phi_e)$, we can express the generalized activating function as

$$S = \mathbf{G}_i : \nabla(\nabla \Phi_e) + (\nabla \cdot \mathbf{G}_i) \cdot \nabla \Phi_e \tag{13}$$

where the colon represents a tensor inner product. This expansion is useful because it illustrates that the terms contributing to the activating function are either products of intracellular conductivities and second derivatives of potential or gradients of conductivity multiplied by gradients of potential. Thus either the first or second derivative of potential can act as a source, but the relative weights of these two terms differ and are determined by tissue characteristics. We can expand this expression for the general, three-dimensional case to observe which products contribute, and obtain

$$\begin{aligned} &= \left(g_x \frac{\partial^2 \Phi_e}{\partial x^2} + g_y \frac{\partial^2 \Phi_e}{\partial y^2} + g_z \frac{\partial^2 \Phi_e}{\partial z^2} + 2g_{xy} \frac{\partial^2 \Phi_e}{\partial x \partial y} + 2g_{xz} \frac{\partial^2 \Phi_e}{\partial x \partial z} + 2g_{yz} \frac{\partial^2 \Phi_e}{\partial y \partial z} \right. \\ &\quad + \frac{\partial g_x}{\partial x} \frac{\partial \Phi_e}{\partial x} + \frac{\partial g_{xy}}{\partial x} \frac{\partial \Phi_e}{\partial y} + \frac{\partial g_{xz}}{\partial x} \frac{\partial \Phi_e}{\partial z} + \frac{\partial g_{xy}}{\partial y} \frac{\partial \Phi_e}{\partial x} + \frac{\partial g_y}{\partial y} \frac{\partial \Phi_e}{\partial y} \\ &\quad \left. + \frac{\partial g_{yz}}{\partial y} \frac{\partial \Phi_e}{\partial z} + \frac{\partial g_{xz}}{\partial z} \frac{\partial \Phi_e}{\partial x} + \frac{\partial g_{yz}}{\partial z} \frac{\partial \Phi_e}{\partial y} + \frac{\partial g_z}{\partial z} \frac{\partial \Phi_e}{\partial z} \right) \end{aligned} \tag{14}$$

In accordance with Eq. 13, all values of g in Eq. 14 refer to intracellular conductivities. Although S appears quite complex in this form, we will consider two simplified cases in which it becomes more tractable.

Constant conductivity tensor

Assuming that the tensor describing conductivity is constant over the entire domain (i.e., fiber orientation and fractional cross-sectional areas are constant), all derivatives of the components of $\mathbf{G}$ are zero. With a proper rotation of the coordinate basis, the conductivity tensor will also be diagonal. Therefore,

$$S = g_x \frac{\partial^2 \Phi_e}{\partial x^2} + g_y \frac{\partial^2 \Phi_e}{\partial y^2} + g_z \frac{\partial^2 \Phi_e}{\partial z^2} \tag{15}$$

where g_x, g_y, g_z, are equal, respectively, to g_l, g_t, g_u, as considered earlier (assuming that fibers run in the x direction). As in the one-dimensional case, second derivatives of external potential act as source terms for the membrane potential response. Furthermore, in the limiting case where g_y and g_z are much smaller than g_x, S can be reduced to Rattay's familiar one-dimensional expression, $\partial^2 \Phi_e / \partial x^2$.

Constant extracellular field

Assuming that the external field strength is constant (i.e., Φ_e varies linearly), a coordinate basis can be defined such that Φ_e varies in only one direction. Defining this to be the x direction,

$$S = \left(\frac{\partial g_x}{\partial x} + \frac{\partial g_{xy}}{\partial y} + \frac{\partial g_{xz}}{\partial z} \right) \frac{\partial \Phi_e}{\partial x} \tag{16}$$

In this case, the applied potential gradient acts as a source, and this source is proportional to gradients in intracellular conductivity. Thus, without a spatially varying intracellular conductivity profile, a uniform field cannot cause tissue to become polarized.

METHODS

To illustrate the salient features of the cases described above, steady-state transmembrane potentials were solved for numerically in a two-dimensional, passive sheet of cardiac tissue. Two models were used in this study: a model with variable intracellular but forced extracellular potentials (approximate model) and an exact, bidomain model in which the equations for intra- and extracellular potentials remained coupled to one another. In the first model, which gives the approximate solution for V_m, the extracellular potential distribution was assumed to be known based on the stimulus conditions, and I_m was replaced with $g_m^{\nu}(\Phi_i - \Phi_e)$ in Eq. 1, where $g_m^{\nu} = 1/R_m^{\nu}$ (in S/mm^3). This equation was discretized, Φ_i was solved for, and V_m was computed from the known Φ_e. For the bidomain case, the same substitution of I_m was performed, but Eqs. 1 and 2 were solved simultaneously. Solving for the transmembrane potentials with both models allowed us to evaluate the assumption that extracellular potentials are not significantly perturbed by the tissue membrane currents.

Both models allow for arbitrary fiber orientation with angle θ (defined in the counterclockwise direction from the x axis) at any point in the tissue. The tissue is assumed to have constant longitudinal and transverse fiber conductivities everywhere in the sheet; thus the local conductivity tensor $\mathbf{G}_f$ is spatially invariant, and Eq. 7 is used to calculate the conductivity tensor at any given location. The rotation matrix $\mathbf{A}$ is given by

$$\mathbf{A} = \begin{bmatrix} \cos\theta & -\sin\theta \\ \sin\theta & \cos\theta \end{bmatrix} \tag{17}$$

and the conductivity tensor $\mathbf{G}$ by

$$\mathbf{G} = \begin{bmatrix} g_l \cos^2\theta + g_t \sin^2\theta & (g_l - g_t)\cos\theta \sin\theta \\ (g_l - g_t)\cos\theta \sin\theta & g_l \sin^2\theta + g_t \cos^2\theta \end{bmatrix} \tag{18}$$

Discretization and creation of linear system

For the solution of Eq. 1 (approximate model) or Eqs. 1 and 2 (exact bidomain), the cardiac sheet was discretized into $n \times m$ elements, and the resulting set of simultaneous linear equations was solved to find the steady-state potential distribution. The number of nodes and the space steps Δx and Δy were different for different simulations considered and will be noted as appropriate in the Results section. First and second derivatives were transformed into finite on-center differences to produce these equations. In the examples considered, the elements of the conductivity tensor are

defined analytically over the whole domain, so that the derivatives of conductivity can be evaluated analytically.

Therefore, the discretized equation for potential in the intracellular domain at node (j, k) is

$$\left[g_x\left(\frac{\phi^i_{j+1,k} + \phi^i_{j-1,k} - 2\phi^i_{j,k}}{\Delta x^2}\right) + g_y\left(\frac{\phi^i_{j,k+1} + \phi^i_{j,k-1} - 2\phi^i_{j,k}}{\Delta y^2}\right) + 2g_{xy}\left(\frac{\phi^i_{j+1,k+1} + \phi^i_{j-1,k-1} - \phi^i_{j-1,k+1} - {}^i_{\phi j+1,k-1}}{\Delta x \Delta y}\right) + \frac{\partial g_x}{\partial x}\left(\frac{\phi^i_{j+1,k} - {}^i_{\phi j-1,k}}{2\Delta x}\right) + \frac{\partial g_y}{\partial y}\left(\frac{\phi^i_{j,k+1} - \phi^i_{j,k-1}}{2\Delta y}\right) + \frac{\partial g_{xy}}{\partial x}\left(\frac{\phi^i_{j,k+1} - \phi^i_{j,k-1}}{2\Delta y}\right) + \frac{\partial g_{xy}}{\partial y}\left(\frac{\phi^i_{j+1,k} - \phi^i_{j-,k}}{2\Delta x}\right) \right] = g^v_m (\phi^i_{j,k} - \phi^e_{j,k}) \quad (19)$$

The system of linear equations that defined the potentials in the tissue was solved with an LU decomposition routine that took advantage of the bandedness and sparseness of the system matrix. All simulations were implemented in MATLAB (The Math Works, Natick, MA) on a Silicon Graphics (Mountain View, CA) workstation.

Boundary conditions and stimulation

In one case, we simulate the response of a thin, two-dimensional sheet of myocardium to a point source of current situated above the center of the tissue in a semiinfinite isotropic extracellular space. We solve the approximate problem in this case, and specify extracellular potentials assuming a $1/r$ falloff in potential from the source, as would occur in an infinite isotropic volume conductor. Because of symmetry, we need only solve for the potentials in one quadrant of the tissue, and we assume that all edges of the sheet are sealed (i.e., current cannot flow off the tissue). To calculate the tissue impulse response in these simulations, we assume the extracellular space is grounded and inject a unitary intracellular current at the origin.

In other cases under consideration, we are interested in examining the response of a region that is assumed to lie in the tissue bulk, far from the electrodes. There, current will distribute between the intra- and extracellular domains such that the fields in both domains are equal if the fiber direction is uniform. The relative magnitudes of these currents are easily calculated from the intra- and extracellular conductivities. In the bidomain model, these "redistributed currents" are applied in both domains along the edges of the tissue that are perpendicular to the direction of the applied field. The tissue edges that run in the orthogonal direction are sealed so that no current flows off these borders. The magnitudes of the applied currents are scaled such that the local potential gradients are both equal to 1-V/cm. In the approximate model, a similar strategy is employed, except that currents need to be specified only in the intracellular domain. Because the potential difference between adjacent extracellular nodes is well defined, the intracellular currents needed to cause a 1-V/cm field are easily computed.

Model parameters

Model parameters are given in Table 1. Intracellular conductivity, membrane conductivity, and surface area-to-volume ratio were chosen in accordance with those used by Sepulveda et al. (1989). The computed intra- and extracellular conductivities assume an intra- to extracellular volume ratio of 0.7/0.3. We assume the extracellular space to be isotropic. Although resistance measurements in tissue have shown that this is probably not the case (Clerc, 1976), we feel that this condition is not truly restrictive and will cause only quantitative differences in our results, because our tissue will have an unequal anisotropy ratio. In the two-dimensional case, Roth has argued that the tissue anisotropy ratio is more important than the anisotropy of either domain per se in determining the response of the tissue to a point stimulus (Roth, 1992). Even though we will simulate conditions different from those examined by Roth (i.e., unbounded volume conductor in Fig. 1 and curving fibers in Fig. 6), the response of our tissue to stimulation should be qualitatively similar to that of tissue with an anisotropic extracellular space, because the anisotropy ratios in the two domains are unequal.

RESULTS

We begin by examining some well-known examples from the cardiac stimulation literature that illustrate the utility of the generalized activating function. After these, we will show results that suggest other ways that cardiac cells in the bulk of the myocardium can be polarized. First, we use the approximate model to simulate the point stimulation of a thin sheet of cardiac tissue. The stimulating cathode lies 50 μm above the tissue in a semiinfinite isotropic conductive medium, and the intracellular space has a conductivity 10 times greater in the longitudinal direction than in the transverse direction. Thus, although the tissue lies in a plane, extracellular potentials fall off in three dimensions, as was the case in Rattay's simulations of a single neuron in an

TABLE 1 Model Parameters

Parameter	Value	Description
g_{li}	2e-4 S/mm	Longitudinal intracellular conductivity
g_{ti}	2e-5 S/mm	Transverse intracellular conductivity
g_{le}	1e-3 S/mm	Longitudinal extracellular conductivity
g_{te}	1e-3 S/mm	Transverse extracellular conductivity
β	200 mm^{-1}	Membrane surface area to tissue volume ratio
$g^v_m = \beta \cdot g_m$	1e-3 S/mm^3	Membrane conductivity

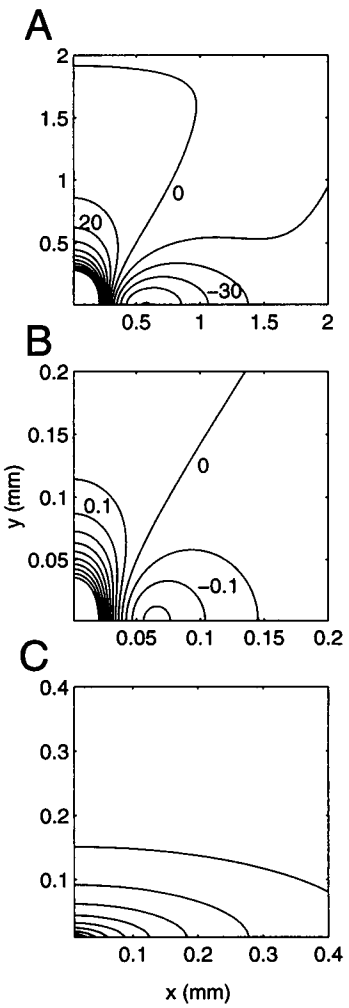

FIGURE 1 Point stimulation of an anisotropic sheet of cardiac tissue. Intracellular conductance is 10 times higher in the x direction than in the y direction, and the stimulating cathode is located 50 μm above the surface in a semiinfinite, isotropic volume conductor. (*A*) Contours of induced transmembrane potentials, in 10-mV incrememts. (*B*) Contours of the generalized activating function, normalized to its peak value, in increments of 0.1. (*C*) Response of the tissue to a unitary current injected at the origin, normalized to its peak value.

unbounded volume conductor. When tissue with such unequal anisotropy is stimulated with a point electrode, a "dog bone" pattern of polarization develops, as is shown in Fig. 1 *A*, which is a contour plot of the resulting transmembrane potential profile. Because of symmetry about the origin, only one quadrant of the tissue is displayed. As has been predicted (Sepulveda et al., 1989; Roth, 1992) and experimentally verified (Neunlist and Tung, 1995; Knisley, 1995; Wikswo et al., 1995) in other studies, the potential induced by the stimulus decays monotonically to zero in the transverse (y) direction, and a region of oppositely polarized tissue (what has been termed the virtual anode) exists in the longitudinal (x) direction. Contours of the corresponding generalized activating function (normalized to its peak value) are displayed in Fig. 1 *B*. This term is defined by Eq. 16, except that the third term is zero since we are only considering a two-dimensional sheet of tissue. The generalized activating function, which defines the virtual sources, resembles the V_m distribution, but the contour lines are clustered much closer to the origin (note the different x and y axis scales in Fig. 1, *A* and *B*). The tissue response, then, which is a convolution of the activating function with the tissue impulse response, is a spatially low-pass filtered version of the activating function. The impulse response, shown in Fig. 1 *C*, decays with distance from the source, so the tissue acts to spread out the charge introduced into the intracellular domain.

Virtual electrodes of opposite polarity result when a point source stimulates unequally anisotropic tissue. However, previous studies indicate that when the tissue is equally anisotropic or isotropic, potential will fall off monotonically from the source and no oppositely polarized regions will exist (Jack et al., 1976; Sepulveda et al., 1989). In Fig. 2 we see that the generalized activating function predicts this phenomenon. The conditions of this simulation are identical to those of Fig. 1, except that here the intracellular transverse (y) conductance is identical to the longitudinal (x) conductance. Fig. 2 *A* displays contours of the induced V_m, which are seen to peak at the origin, where the point source is located, and fall off monotonically in all directions. The generalized activating function contours are shown in Fig. 2 *B*, and again we observe that the tissue response is a low-pass filtered version of this term. Fig. 2, *C* and *D*, illustrates why the generalized activating function predicts oppositely polarized regions when the tissue is unequally anisotropic, but only one polarity of V_m when the tissue is isotropic. From Eq. 15, we see that the source term has two components, $g_x\partial^2\Phi_e/\partial x^2$ and $g_y\partial^2\Phi_e/\partial y^2$, which are plotted in Fig. 2, *C* and *D*, respectively. Surface plots are displayed instead of the contour plots used previously, because these can be visually summed more easily. The two partial second derivatives of potential contribute to the activating function, but their relative contributions depend on the longitudinal and transverse conductivities. When they are equally weighted and summed, the oppositely polarized virtual sources in the x and y directions will mask each other such that the overall activating function becomes the monopolar source shown in Fig. 2 *B*. If they are unequally weighted, though, sources of opposite polarity will exist side by side. This is apparent when the extreme case of unequal anisotropy, complete transverse uncoupling, is considered. This situation leads to the most pronounced dog-bone pattern (Roth, 1992) and is equivalent to setting either g_x or g_y to zero, so that the activating function consists of only one of the two terms.

A second mechanism of stimulation that is well studied in the cardiac literature is the "sawtooth" polarization pattern caused by resistive discontinuities at gap junctions between adjacent cells (Plonsey and Barr, 1986a; Krassowska et al., 1987; Cartee and Plonsey, 1992). Fig. 3 shows that this mechanism can be understood in terms of the generalized activating function as well. As schematically illustrated in

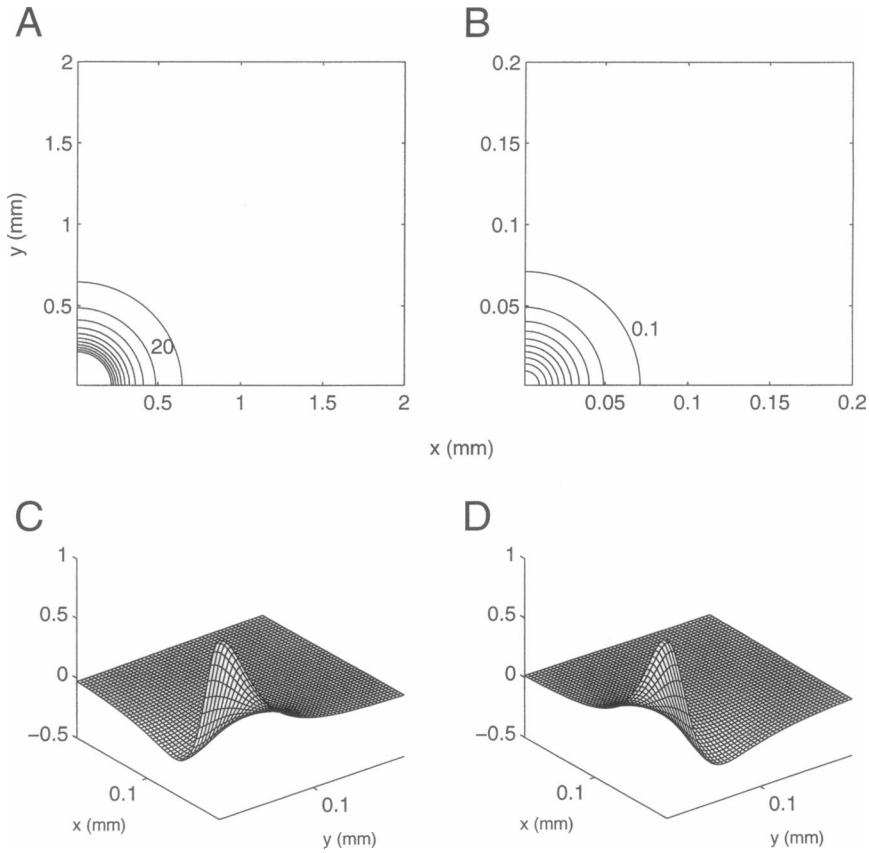

FIGURE 2 Point stimulation of an isotropic sheet of tissue. Conditions are identical to those in Fig. 1, except that intracellular x and y conductances are equal. (*A*) Contours of induced transmembrane potentials, in 10-mV incrememts. (*B*) Contours of the generalized activating function, normalized to its peak value, in increments of 0.1. (*C*) Surface plot of the normalized x-component of the generalized activating function, $g_x\partial^2\Phi_e/\partial x^2$. (*D*) Surface plot of the normalized y component of the generalized activating function, $g_y\partial^2\Phi_e/\partial y^2$.

Fig. 3 *A*, we impose a uniform electric field on a sheet of tissue with a uniform fiber direction, and periodically vary the longitudinal conductivity such that the conductance is decreased by a factor of 1000 every 100 μm. Both the field and the fibers are assumed to be oriented along the x direction. The generalized activating function in this case reduces to one term, $\partial g_x/\partial x \cdot \partial\Phi_e/\partial x$, because the field is uniform (all second derivatives are zero), and all off-diagonal terms in the conductivity tensor are zero. This remaining term is nonzero only where the conductance changes: it is a positive virtual source where the conductance decreases (in the direction of the field), and a negative source where the conductance increases. Thus every location with depressed conductivity represents a dipole source, as illustrated in Fig. 3 *B*. The response of the tissue to this stimulus is displayed in Fig. 3 *C*, with the solid lines displaying the approximate solution and the dotted lines the exact bidomain solution. Here we only show a cross section of the sheet, because all sections across the transverse direction are equivalent. The exact and approximate solutions are so close in this case that the dotted lines are obscured by the solid lines. The pattern that develops is the familiar "sawtooth," which can now be thought of as a filtered version of the distribution of periodic dipole sources. The maximum and minimum potentials that develop are 4.53 mV and -4.53 mV, respectively, for a 1-V/cm field.

In Fig. 4, we consider another situation in which discontinuities in conductivity can induce secondary sources when a uniform field is applied to tissue. Fig. 4 *A* displays tissue containing a region where intracellular conductivity is depressed, as might occur if cells are ischemic. We assume that a uniform field is oriented as shown and that both longitudinal and transverse conductivities are decreased by a factor of 3 throughout the region. In this case the activating function is again $\partial g_x/\partial x \cdot \partial\Phi_e/\partial x$, so a positive virtual source is produced at the left edge and a negative source at the right edge of the depressed region, as seen in Fig. 4 *B*. The magnitudes of the sources are proportional to the applied field and to the change in conductivity, and the sources are constant across the transverse extent of the region. The tissue response is displayed in Fig. 4 *C*, and again we show the approximate solution with solid contour lines and the bidomain solution with dotted lines. With the 50 μm $\times$ 100 μm depressed region that is simulated, and a 1-V/cm field, the maximum depolarization/hyperpolarization produced is $\pm$3.91 mV with the bidomain solution and $\pm$4.20 mV in the approximate model. In Fig. 4 *D* we show the response of the sheet when the conductivity in the depressed region is zero, as would occur if this region represented necrotic tissue or a hole in the tissue, such as, for example, a break caused by a blood vessel. The change in conductivity along the edge of this hole is greater than in the previous example, which leads to stronger sources along the edges of the hole. Consequently, the maximum potentials induced in the tissue are $\pm$9.46 mV (full bidomain) and $\pm$9.45 mV (approximate).

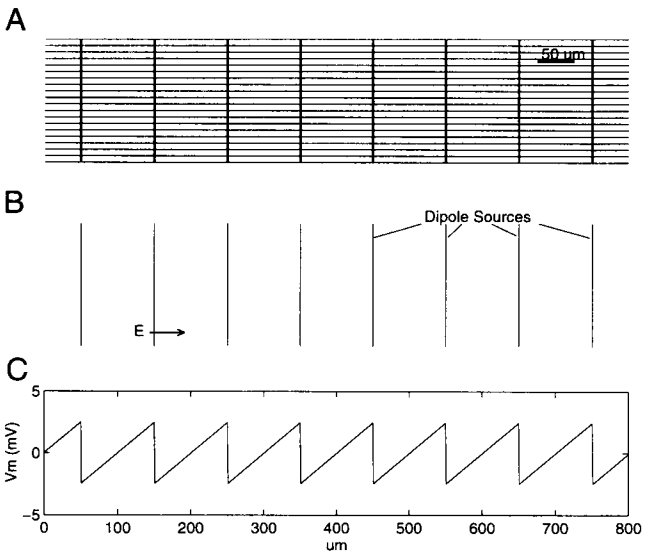

FIGURE 3 Stimulation of a sheet of tissue with periodically varying conductivity. (*A*) Geometry. Intracellular conductivity is reduced by a factor of 1000 every 100 μm, as indicated by the thick vertical lines. A uniform 1-V/cm field is applied to the tissue as shown. (*B*) Generalized activating function. Each gap junction, or periodic reduction in conductivity, causes a dipole source. (*C*) Tissue response. The approximate solution (*solid lines*) masks the bidomain solution (*dotted lines*).

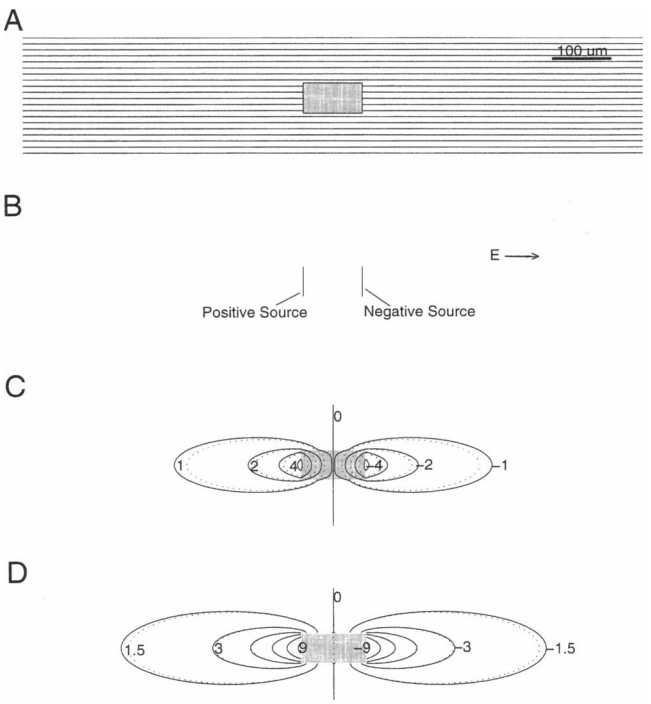

FIGURE 4 Stimulation of a sheet of tissue containing a region of depressed conductivity. (*A*) Geometry. Intracellular conductivity is depressed in the shaded region, and a 1-V/cm field is applied as shown. (*B*) Generalized activating function. A positive source is produced along the left edge of the shaded region, and a negative source along the right edge. (*C*) Contours of induced V_m (in mV) for the approximate solution (*solid lines*) and the bidomain solution (*dotted lines*) when conductance in the shaded region is decreased by a factor of 3. (*D*) Contours of the tissue response when conductance in the shaded region is zero.

A change in fiber diameter is another condition that could lead to membrane polarization in the tissue bulk. Qualitatively, when a fiber narrows, current is forced across the membrane because of the increased resistance in the longitudinal direction, and the membrane near the narrowing is depolarized. A two-dimensional simulation of this is illustrated in Fig. 5. If we consider a 500-μm-wide tissue strip that narrows to a width of 250 μm over 1 mm, as indicated in Fig. 5 *A*, positive virtual sources are produced along the edges of the narrowing, as shown in Fig. 5 *B*. The V_m profiles produced in this narrowing strip are shown with solid and dotted lines in Fig. 5 *C*, from which we observe that maximum depolarizations of 16.37 mV (bidomain) and 16.38 mV (approximate) are produced from a 1-V/cm stimulus field.

As a final example, we consider the polarization pattern that results when a uniform field is applied to fibers that are curving around an anatomical obstacle. Fig. 6 *A* schematically illustrates half of the region of tissue that we are simulating. If we flip the structure in Fig. 6 *A* around its left edge to produce the left half of the region, we see that the domain under consideration contains a long, oval-shaped hole with fibers curving around it. Current is applied at the left border of the tissue and is removed at the right edge. Because of the symmetry about the center of the obstacle with the field oriented as shown, each location on the half of the tissue that is displayed is exactly oppositely polarized from its "mirror image" on the other side. Fig. 6 *B* displays contours of the generalized activating function that is computed with the assumption that the extracellular field is uniform everywhere in the tissue. A hyperpolarizing source is produced along the edge of the obstacle, which is similar to the effect of the hole shown in Fig. 4 *D*, and the fiber curvature produces a depolarizing activating function that peaks near the edge of the obstacle, and where the fibers have become perpendicular to the field. Thus the smooth changes in conductivity due to fiber curvature cause distributed sources, and the discontinuity in conductivity at the edge of the obstacle also causes polarization. A smaller radius of curvature causes larger sources, and these sources reach a maximum where the fiber is orthogonal to the field. The transmembrane voltages induced by the stimulus are shown in Fig. 6 *C* for the approximate (*solid lines*) and bidomain (*dotted lines*) solutions. The two solutions are qualitatively similar, with a hyperpolarized region near the obstacle edge and a graded depolarization in the remainder of the tissue. Although the locations of the peak hyper- and depolarizations are very close, the magnitudes of these peaks, -3.06 and $+10.35$ mV for the approximate and -2.22 and $+7.27$ for the exact bidomain model, differ by as much as 42%. Thus this approximate solution captures the salient features of the true solution but is quantitatively inaccurate.

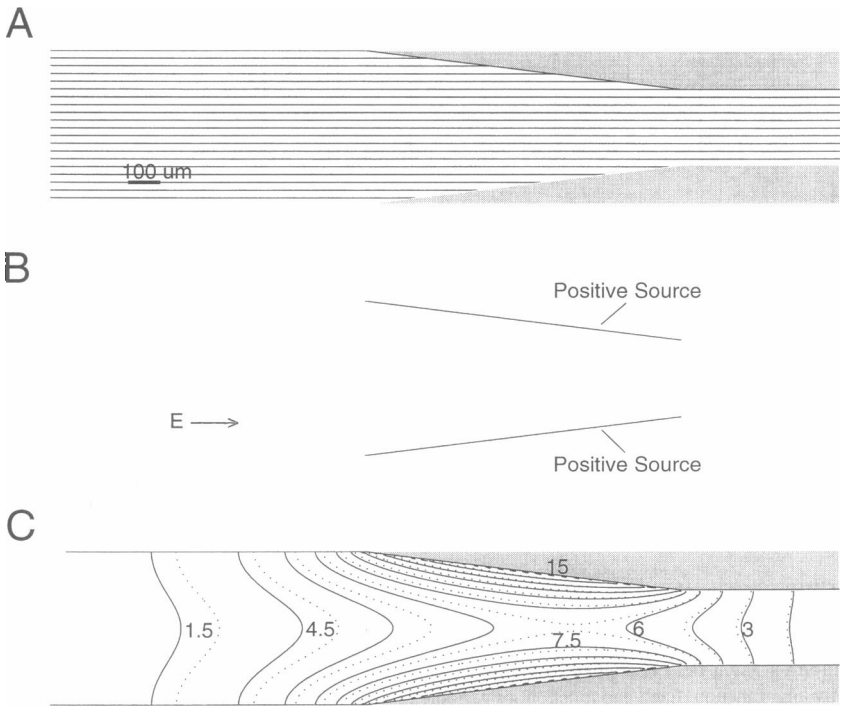

FIGURE 5 Membrane polarizations caused by fiber narrowing. (*A*) Geometry. A 500-μm-wide fiber narrows to 250 μm over 1 mm, and a 1-V/cm field is applied along the fiber's longitudinal axis. (*B*) Generalized activating function. As the fiber narrows, positive sources are produced along the edges of the fiber. (*C*) Tissue response. Contours of the induced V_m (in mV) for the approximate (*solid lines*) and exact bidomain (*dotted lines*) solutions.

A more accurate approximate solution could presumably be obtained if a better estimate of the extracellular potentials were used. Because in this example we are interested in extracellular potentials that develop in the tissue bulk and without the influence of tissue membrane currents, we hypothesized that one way to obtain such an estimate would be to solve for a primary potential distribution that satisfies

$$\nabla \cdot [(\mathbf{G}_i + \mathbf{G}_e)\nabla\Phi_e^p] = 0 \qquad (20)$$

Equation 22 is Laplace's equation for a parallel combination of intra- and extracellular conductivities, which would be appropriate for potentials that develop in a region where currents are in a quasiequilibrated distribution between the two domains. Φ_e^p and the transmembrane potentials that result from it were computed and compared against those computed assuming a uniform field. The V_m contours for this approximate solution are shown in Fig. 6 D (*solid lines*) along with the exact bidomain solution (*dotted lines*). In contrast to the approximate solution displayed in Fig. 6 *C*, in this panel the approximate and bidomain contours match up extremely well. To compare the accuracy of the two approximate solutions, we computed the average root-mean-square error over all of the nodes ($\bar{E}_{RMS}$) between each approximate solution and exact bidomain solution. For the case of the curved fibers (Fig. 6), $\bar{E}_{RMS}$ was 0.448 mV assuming a uniform field, and 0.0063 mV when Eq. 20 was solved. Thus a much more accurate approximate solution was obtained by solving Eq. 20 and using this as our Φ_e^p distribution. We also compared the two approximate solutions for the examples considered earlier and present the errors for the uniform field and "parallel combination" solutions as follows. For the sawtooth pattern shown in Fig. 3, $\bar{E}_{RMS}$ is 0.0026 and 0.88 mV, respectively, showing substantially larger error when Eq. 20 was used. For the region of depressed conductivity shown in Fig. 4, the errors are 0.042 and 0.031 mV when conductivity is reduced by a factor of 3 (Fig. 4 *C*) and 0.046 and 0.038 mV when conductivity is zero in the depressed region (Fig. 4 *D*). Finally, for the narrowing fiber shown in Fig. 5, $\bar{E}_{RMS}$ is 0.25 and 0.15 mV, respectively.

DISCUSSION

In this study we have identified a new mathematical expression that describes the sources, or virtual electrodes, that drive changes in transmembrane potential when cardiac muscle is stimulated by applied electric fields. In general, source terms exist where the applied field changes or intracellular conductivity varies. In simulations of the steady-state voltage distribution in a two-dimensional sheet of cardiac tissue, we have shown that this expression, which we term the generalized activating function, can predict and lend understanding to such well-known phenomena as the dog-bone and sawtooth patterns of polarization. It can also be used to postulate additional ways that cells can be polarized in the tissue bulk, such as ischemic, necrotic, or missing cells, changes in fiber diameter, or fiber curvature.

This analysis can help to unify much of the previous work in the field of cardiac electrical stimulation. In the past, investigators interested in these questions have tended to divide the effects of electrical stimuli into categories and treat various induced membrane polarizations as if they occurred by different mechanisms. For instance, Krassowska and co-workers, in considering tissue with periodi-

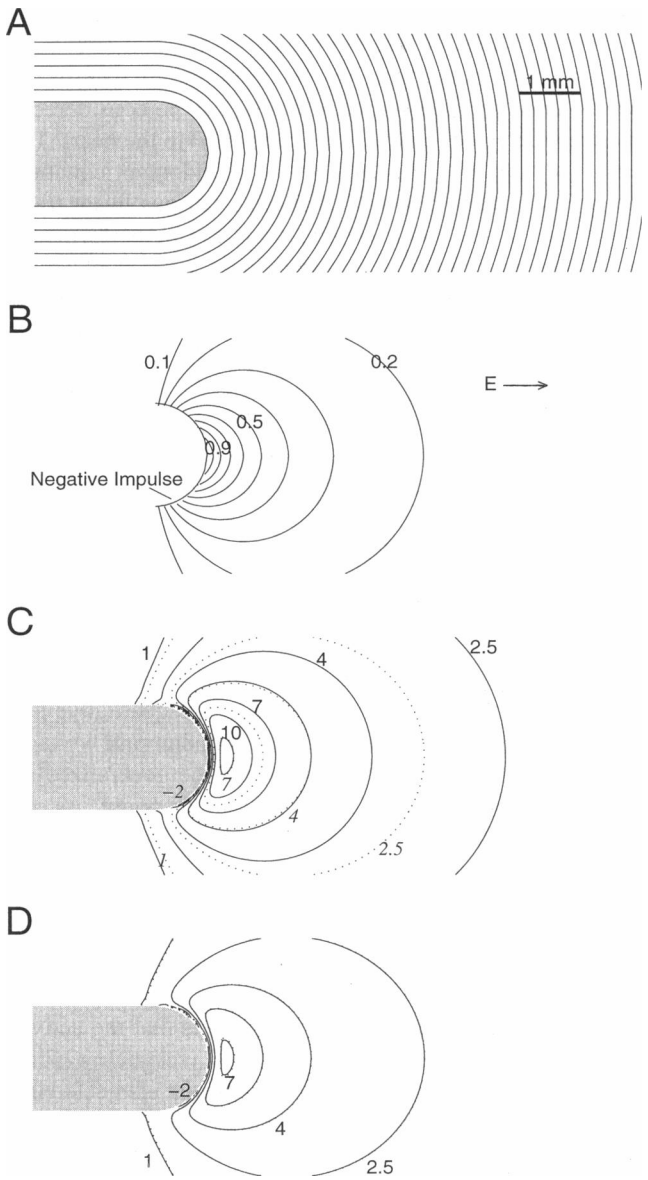

FIGURE 6 Stimulation of fibers curving around an obstacle. (*A*) Geometry. Intracellular conductivity is zero in the shaded region, the applied field is oriented as shown, and the fibers curve around the obstacle as shown. Where the muscle fibers curve, the fiber angle θ is described by $\theta = -\tan^{-1}(x/y)$. (*B*) Generalized activating function. A hyperpolarizing source is produced along the edge of the obstacle, and distributed depolarizing sources arise because of fiber curvature. Contours of this component are plotted, normalized to the function's peak value. (*C*) Tissue response. Contours of the induced V_m (in mV) for the approximate (*solid lines*) and exact bidomain (*dotted lines*) solutions. Contour values on the top half of the panel apply to the solid lines, and the values on the bottom half (in italics) apply to the dotted lines. This approximate solution assumes that a uniform 1-V/cm field is applied to the tissue. (*D*) Tissue response with an alternative approximate solution. Contours of the induced V_m for the approximate (*solid lines*) and bidomain (*dotted lines*) solutions. See text for details of the approximate solution method.

cally varying conductivity, defined two space scales and solved the "global" and "local" problems separately (Krassowska et al., 1987, 1990); Trayanova and Roth speak of "continuous" and "discrete" mechanisms for stimulation (Trayanova and Roth, 1993); Fishler et al. discuss "near-field" and "far-field" effects (Fishler et al., 1996); Plonsey and Barr refer to "primary" and "secondary" sources (Plonsey and Barr, 1986a,b); and Trayanova et al. differentiate between "surface" and "bulk" polarizations (Trayanova et al., 1993). The generalized activating function provides a formalism by which one can predict various effects of a stimulus without having to separate these mechanisms into classifications. For example, when a uniform field is applied to a discontinuous, one-dimensional cardiac fiber, the polarizations that occur within a few space constants of the stimulating electrodes are caused by the combination of the field and the large changes in conductance at the fiber's sealed ends, whereas the sawtooth oscillations in potential that dominate in the center of the fiber are driven by the product of the field strength and the changes in intracellular conductance at the gap junctions between adjacent cells.

Furthermore, the formulation that we have introduced provides, as far as we are aware, the most general expression derived to date that applies the concept of the activating function to the study of cardiac tissue. Other researchers have used this idea to lend understanding to their studies, but, without a more inclusive formula, these have been applicable only under specific conditions. Roth has used Rattay's activating function to draw parallels between the cardiac dog-bone potential pattern and effects observed during neuronal stimulation (Roth, 1992); Trayanova et al. have derived one-dimensional formulas that help explain how fiber curvature and fiber branching cause potentials to develop in the bulk of their spherical heart model (Trayanova et al., 1993); and Keener has recently noted that an expression which includes the effects of spatially varying conductivity acts as a source term in his study of sawtooth effects in a one-dimensional strand of muscle (Keener, 1996). Our approach is comprehensive and can bring together these disparate applications of the notion of the activating function.

Here we should point out that we give the term "virtual electrode" a meaning that differs from that given to it in previous works (Wikswo et al., 1991, 1995; Knisley et al., 1994). The term "virtual cathode" has been used to refer to the region of tissue that is depolarized, if any exists, when excitable tissue is stimulated with an extracellular electrode. However, we believe the term "virtual cathode" should indicate the region where a depolarizing source is produced, delineated by the activating or forcing function, which, as our simulations show, is not the same as the region that is eventually depolarized. The previous definition makes sense from an experimental perspective, because sources cannot be directly measured, but on theoretical grounds we consider it more accurate to define the virtual electrode as the source that acts to polarize the membrane, rather than the polarization that is produced. This is a subtle, but nonetheless important, distinction.

Role of the generalized activating function

As we have seen above, when resting cardiac tissue is electrically stimulated, the generalized activating function, defined by $\nabla \cdot (\mathbf{G}_i \nabla \Phi_e)$, describes the sources that drive changes in transmembrane potential or, in other words, delineates the locations and magnitudes of the virtual electrodes. When we expand this term for arbitrary, possibly spatially varying, conductivity (Eq. 14), we observe that membrane potentials can develop if the second derivative of extracellular potential is nonzero, or if the applied field is uniform and gradients in intracellular conductivity exist. The reasons for this can be understood if we consider what the circumstances must be for transmembrane potential *not* to develop. If $V_m = 0$, then we must have $\Phi_i = \Phi_e$, and, furthermore, any gradient in extracellular potential must be matched in the intracellular space. If the extracellular field is uniform and intracellular conductivity is unchanging in space, then Φ_i can match Φ_e by way of a constant intracellular current density. However, if the extracellular field varies in space, then the intracellular current density must change to match this new extracellular field and maintain zero transmembrane potential. Intracellular current density can change only by way of a membrane current, and this current will create a voltage where it crosses the membrane. Therefore, a transmembrane potential must develop if the applied field is nonuniform.

On the other hand, if the extracellular field is constant, potentials can still develop in regions where the intracellular conductivity is changing. In regions where V_m is zero, current has divided (redistributed) between the intracellular and extracellular spaces such that the potential gradients in the two domains are equal. If the intracellular current encounters a region where conductance changes, the fractions of the total current in each of the two domains will no longer be appropriate. Current will cross the membrane to redistribute the current, and a nonzero transmembrane potential will result.

A corollary of the discussion above is that transmembrane potentials can develop only if the anisotropy ratios between the intra- and extracellular spaces are not equal everywhere. This can be seen by examining the primary extracellular potential distributions that we have chosen: each satisfies either $\nabla \cdot (\mathbf{G}_e \nabla \Phi_e^p) = 0$ or $\nabla \cdot [(\mathbf{G}_i + \mathbf{G}_e) \nabla \Phi_e^p] = 0$. When tissue is equally anisotropic, the two conductivity tensors are scalar multiples of one another. If we substitute $\mathbf{G}_e = k\mathbf{G}_i$ into either of the above equations, we see that the generalized activating function, $\nabla \cdot (\mathbf{G}_i \nabla \Phi_e^p)$, is zero everywhere. Fig. 6 examines the effects of fiber curvature under unequally anisotropic conditions, so to verify that the above reasoning is correct, we computed the response of this model under the condition of equal anisotropy. For the approximate solution we numerically solved $\nabla \cdot (\mathbf{G}_e \nabla \Phi_e^p)$ and used this potential distribution (no longer a uniform field) in our model. As expected, significant potentials did not develop in the bulk of the tissue but only arose because of the anatomical obstacle in either the approximate or exact bidomain model (results not shown).

It should be noted that the expression we have derived is not the only possible source term that can be considered to operate when electrical stimuli are applied to the heart. This term is unique to the particular set of bidomain equations that we have chosen to work with, but various linear transformations of the bidomain equations can be performed to yield different equivalent governing equations (Hooke et al., 1994). These different sets of equations will lend themselves to manipulations that can yield alternative expressions for source terms (e.g., Goel and Roth, 1994). Furthermore, if the sources for a variable besides transmembrane potential, such as intracellular potential, are desired, then different expressions will result, as have been derived for the case of axonal stimulation (Rubinstein and Spelman, 1988; Rubinstein, 1991). Nevertheless, we feel that our generalized activating function serves as a good intuitive source term because it describes the initial change in V_m and because it is a logical extension of the one-dimensional activating function as originally proposed by Rattay (1986).

Even though we have only examined steady-state phenomena in this study, we can gain at least a qualitative idea of the temporal evolution of tissue tranmembrane voltages by examining the relationship between the generalized activating function (sources) and the tissue response. As others have shown with Rattay's activating function in the one-dimensional case (Warman et al., 1992; Neunlist and Tung, 1995; Plonsey and Barr, 1995), the tissue response can be considered a convolution of the generalized activating function with the tissue impulse response if the tissue is shift-invariant. Thus all time dependence is contained in the impulse response term because we assume that the activating function does not change in time (see below for a discussion of this assumption). When current is injected into passive tissue, potentials first develop in tissue very close to the source, and over time, charge diffuses to more peripheral tissue, causing potentials to develop away from the source. Thus, near the beginning of the stimulus, the potential distribution will resemble the activating function, and at longer and longer times, as the impulse response spreads out, the potentials induced in the tissue become more smoothed out or low-pass filtered. Although we did not specifically examine time-dependent phenomena in this study, this intuition is consistent with other studies that have examined the temporal evolution of dog-bone (Roth and Trayanova, 1993; Roth and Wikswo, 1994) and sawtooth (Cartee and Plonsey, 1992; Fishler, 1997) polarization patterns.

In the most general case, where the tissue impulse response varies from location to location, a convolution integral cannot be used to compute the tissue response (Figs. 3–6). To compute the approximate time-varying solution in this case, Eq. 4 must be discretized and V_m computed at each time step based on the time-invariant activating function and the spatial distribution of V_m at the previous time step. Even though this simulation would be more computa-

tionally difficult than a convolution integral, it would still be less costly than solving the full bidomain system.

Exact versus approximate solutions

As discussed in the Theory section, if the extracellular potential distribution caused by the applied stimulus is known, then the generalized activating function describes the source term for V_m exactly. In general, though, we cannot determine the exact potentials without considerable effort and would prefer to use the assumed extracellular fields, or $\nabla\Phi_e^p$, to estimate the sources. In the examples we have presented above, we were able to identify Φ_e^p distributions that provided accurate approximate solutions. No qualitative differences were observed between the exact and approximate solutions in the cases that we considered.

In many of our simulations we were able to easily estimate an accurate extracellular potential distribution because the circumstances of the stimulation suggested a simple answer for this distribution (i.e., a uniform field). In the example of Fig. 6, however, where fiber direction was variable in the sheet, our initial estimate of a uniform field provided an approximate solution that was qualitatively similar to the exact solution but was quantitatively inaccurate. In this instance, we had to first solve Laplace's equation with a parallel combination of intra- and extracellular conductivities (Eq. 20) to determine the primary potential distribution, and then use these potentials to obtain an accurate estimate of V_m. This method is computationally equivalent to solving two approximate problems, which is nevertheless still easier than solving the full bidomain system.

When we solved Eq. 20 to determine the primary extracellular potentials and used this distribution to solve the approximate problem, the error decreased greatly for the case of curved fibers considered in Fig. 6, increased significantly for the sawtooth pattern shown in Fig. 3, and decreased slightly in all other cases considered. This approach of first solving Laplace's equation for the parallel combination of intra- and extracellular conductivities seems to provide a more accurate solution in situations where the conductivity is changing gradually and currents may be more fully redistributed but not work as well when the conductivity changes abruptly. Further investigation is needed to determine the best way of estimating the primary potential distribution for an arbitrary fiber geometry.

Because our simulations only apply to specific geometries and represent passive conditions, it is worthwhile to consider other instances in which the approximate solution may be more or less accurate. The restrictiveness of the extracellular space should affect how much the membrane currents perturb the applied extracellular fields, with a given current producing larger fields in more confined spaces. Our intra- to extracellular volume ratio of 0.7/0.3 is typical of that used by other investigators and is consistent with the experimental measurements of Kléber and Riegger (1987). To obtain an order of magnitude estimate of the perturbations in extracellular fields caused by nonlinear and time-dependent membrane currents, we can consider the extracellular fields caused by a propagating wavefront. This should represent an upper limit because large current densities flow across the cell membrane during the depolarization phase of the action potential. Extracellular potentials during propagation have been measured (Knisley et al., 1991) and computed (Henriquez and Plonsey, 1990; Roth, 1991), both on the surface of a slab of tissue and in the deeper layers of the muscle. These potentials reach maximum amplitudes on the order of 50 mV peak to peak deep within the tissue. If we assume that depolarized tissue lies ~1–2 mm from excitable tissue at the leading edge of a cardiac wavefront, then the maximum fields produced by the membrane currents should be on the order of 25–50 mV/mm, or 0.2–0.5 V/cm. These fields will be at least an order of magnitude less than the primary fields applied during a defibrillation shock, and will be even smaller near the surface of cardiac tissue.

Applications to defibrillation

Even though there is still disagreement over the mechanisms by which a strong electrical stimulus revives a fibrillating heart, defibrillation is generally acknowledged to be impossible without changes in the transmembrane potentials of cells in a significant majority of the myocardium (Dillon, 1992). Thus the question of how cells away from the electrodes become polarized has been of major importance in defibrillation research, and as noted in previous sections, many different mechanisms have been proposed. A related question concerns whether the extracellular potential gradient (electric field) or the gradient of the potential gradient is the more important factor in determining whether cells are affected by a given stimulus. This work shows that second derivatives in extracellular potential cause sources that are weighted by the tissue conductivity (Eq. 15), and as illustrated in Fig. 1 and Fig. 2, the relative contributions of these weights influence the eventual shape of the generalized activating function. In this respect our generalized activating function differs from Rattay's original formulation, as he neglected the conductivity term in his definition. Sources due to uniform extracellular fields are weighted by gradients in intracellular conductivity (Eq. 16). Thus both gradients in extracellular potential and changes in these extracellular fields can act to cause polarization of cardiac tissue, but the tissue architecture is equally important in determining the polarities and relative magnitudes of the sources. Future work will be necessary to assess the relative contributions of these two source terms.

Some leading theories of defibrillation mechanisms postulate that a minimum extracellular potential gradient must be produced throughout the myocardial volume for the shock to succeed (Ideker et al., 1994). Because of this, current-day research on electrode configurations focuses on

the potential gradients produced in the myocardial volume and aims to create a potential distribution such that the electric field is as uniform as possible and above a certain value everywhere in the heart (Karlon et al., 1993; Panescu et al., 1995; Schmidt and Johnson, 1995). Large computer models of the human thorax are constructed to solve Laplace's equation (Johnson et al., 1992), or, on the experimental side, epicardial sock electrodes and intramural plunge electrodes are used to measure the potentials caused by the shock for a given set of electrode characteristics (Tang et al., 1992; Wharton et al., 1992). Our research suggests additional steps that can be taken to improve this process and make it more biophysically based. With the extracellular potentials measured in an experiment or computed from a torso model and some estimate of fiber structure, the generalized activating function can be used to calculate the sources. If desired, the membrane polarizations caused by the shock can then be computed based on this source term and an assumed tissue impulse response. By following this procedure, an investigator would know not only the extracellular fields, but would also have an estimate of the changes in V_m caused by a given stimulus. To assess whether a given shock would defibrillate, more information, such as the action potential prolongation, or the induced spatial excitatory response, would be needed, but simply having an estimate of the induced V_ms would represent a significant improvement over the methods currently used.

CONCLUSIONS

In this study we have shown that the concept of the activating function, which has been a useful tool in the study of neuronal stimulation for many years, can be generalized and applied to the multidimensional problem of cardiac electrical stimulation. The generalized activating function that we have derived represents the virtual electrodes that are present during a given electrical stimulus and describes how transmembrane potentials will initially change when the stimulus is applied. Sources can be due to extracellular fields or gradients in these fields. However, the tissue characteristics are also important in that they determine the relative influence of a given source. In passive, steady-state, two-dimensional computer simulations, we have shown that the generalized activating function can predict many mechanisms of membrane polarization. If the extracellular potentials caused by a given stimulus and the tissue architecture can be reliably estimated, which should often be the case when strong electrical stimuli are applied to the heart, then the generalized activating function provides a method for assessing the transmembrane potentials caused by a shock with reduced effort, greater insight, and a relatively high degree of accuracy.

This research was supported in part by grant HL-42866 from the National Institutes of Health to LT.

REFERENCES

Altman, K. W., and R. Plonsey. 1990. Analysis of excitable cell activation: relative effects of external electrical stimuli. *Med. Biol. Eng. Comput.* 28:574–580.

Cartee, L. A., and R. Plonsey. 1992. The effect of cellular discontinuities on the transient subthreshold response of a one-dimensional cardiac model. *IEEE Trans. Biomed. Eng.* 39:260–270.

Clerc, L. 1976. Directional differences of impulse spread in trabecular muscle from mammalian heart. *J. Physiol. (Lond.).* 255:335–346.

Dillon, S. M. 1992. Synchronized repolarization after defibrillation shocks: a possible component of the defibrillation process demonstrated by optical recordings in the rabbit heart. *Circ. Res.* 85:1865–1878.

Durand, D. M. 1995. Electric stimulation of excitable tissue. *In* The Biomedical Engineering Handbook. J. D. Bronzino, editor. CRC Press, Boca Raton, FL. 229–251.

Fishler, M. G. 1997. The transient far-field response of a discontinuous one-dimensional cardiac fiber to subthreshold stimuli. *IEEE Trans. Biomed. Eng.* 44:10–18.

Fishler, M. G., E. A. Sobie, L. Tung, and N. V. Thakor. 1996. Modeling the interaction between propagating cardiac waves and monophasic and biphasic field stimuli—the importance of the induced spatial excitatory response. *J. Cardiovasc. Electrophysiol.* 7:1183–1196.

Goel, V., and B. J. Roth. 1994. Approximate analytical solutions to the bidomain equations describing electrical activity in cardiac tissue. *In* Proceedings of the 13th Southern Biomedical Engineering Conference, Washington, DC. J. Vossoughi, editor. 967–970.

Henriquez, C. S. 1993. Simulating the electrical behavior of cardiac tissue using the bidomain model. *Crit. Rev. Biomed. Eng.* 21:1–77.

Henriquez, C. S., and R. Plonsey. 1990. Simulation of propagation along a cylindrical bundle of cardiac tissue. II. Results of simulation. *IEEE Trans. Biomed. Eng.* 37:861–875.

Hooke, N., C. S. Henriquez, P. Lanzkron, and D. Rose. 1994. Linear algebraic transformations of the bidomain equations: implications for numerical methods. *Math. Biosci.* 120:127–145.

Hunter, P. J., P. M. Nielsen, B. H. Smaill, I. J. LeGrice, and I. W. Hunter. 1992. An anatomical heart model with applications to myocardial activation and ventricular mechanics. *Crit. Rev. Biomed. Eng.* 20:403–426.

Ideker, R. E., P. D. Wolf, and A. S. L. Tang. 1994. Mechanisms of defibrillation. *In* Defibrillation of the Heart: ICDs, AEDs, and Manual. W. A. Tacker, Jr., editor. Mosby, St. Louis. 15–45.

Jack, J. J. B., D. Noble, and R. W. Tsien. 1976. Electric Current Flow in Excitable Cells. Oxford University Press, Oxford.

Johnson, C. R., R. S. MacLeod, and P. R. Ershler. 1992. A computer model for the study of electrical current flow in the human thorax. *Comput. Biol. Med.* 22:305–323.

Karlon, W. J., S. R. Eisenberg, and J. L. Lehr. 1993. Effects of paddle placement and size on defibrillation current distribution: a three-dimensional finite element model. *IEEE Trans. Biomed. Eng.* 40: 246–255.

Keener, J. P. 1996. Direct activation and defibrillation of cardiac tissue. *J. Theor. Biol.* 178:313–324.

Kléber, A. G., and C. B. Riegger. 1987. Electrical constants of arterially perfused rabbit papillary muscle. *J. Physiol (Lond.).* 385:307–324.

Knisley, S. B. 1995. Transmembrane voltage changes during unipolar stimulation of rabbit ventricle. *Circ. Res.* 77:1229–1239.

Knisley, S. B., B. C. Hill, and R. E. Ideker. 1994. Virtual electrode effects in myocardial fibers. *Biophys. J.* 66:719–728.

Knisley, S. B., T. Maruyama, and J. W. Buchanan, Jr. 1991. Interstitial potential during propagation in bathed ventricular muscle. *Biophys. J.* 59:509–515.

Krassowska, W., D. W. Frazier, T. C. Pilkington, and R. E. Ideker. 1990. Potential distribution in three-dimensional periodic myocardium. Part II. Application to extracellular stimulation. *IEEE Trans. Biomed. Eng.* 37:267–284.

Krassowska, W., T. C. Pilkington, and R. E. Ideker. 1987. The closed form solution to the periodic core-conductor model using asymptotic analysis. *IEEE Trans. Biomed. Eng.* 34:519–531.

McNeal, D. R. 1976. Analysis of a model for excitation of myelinated nerve. *IEEE Trans. Biomed. Eng.* 23:329–337.

Neu, J. C., and W. Krassowska. 1993. Homogenization of syncytial tissues. *Crit. Rev. Biomed. Eng.* 21:137–199.

Neunlist, M., and L. Tung. 1995. Spatial distribution of cardiac transmembrane potentials around an extracellular electrode: dependence on fiber orientation. *Biophys. J.* 68:2310–2322.

Nielsen, P. M., I. J. Le Grice, B. H. Smaill, and P. J. Hunter. 1991. Mathematical model of geometry and fibrous structure of the heart. *Am. J. Physiol.* 260: H1365–H1378.

Panescu, D., J. G. Webster, W. J. Tompkins, and R. A. Stratbucker. 1995. Optimization of cardiac defibrillation by three-dimensional finite element modeling of the human thorax. *IEEE Trans. Biomed. Eng.* 42: 185–192.

Plonsey, R., and R. C. Barr. 1986a. Effect of microscopic and macroscopic discontinuities on the response of cardiac tissue to defibrillating (stimulating) currents. *Med. Biol. Eng. Comput.* 24:130–136.

Plonsey, R., and R. C. Barr. 1986b. Inclusion of junction elements in a linear cardiac model through secondary sources: application to defibrillation. *Med. Biol. Eng. Comput.* 24:137–144.

Plonsey, R., and R. C. Barr. 1995. Electric field stimulation of excitable tissue. *IEEE Trans. Biomed. Eng.* 42:329–336.

Rattay, F. 1986. Analysis of models for external stimulation of axons. *IEEE Trans. Biomed. Eng.* 33:974–977.

Rattay, F. 1988. Modeling the excitation of fibers under surface electrodes. *IEEE Trans. Biomed. Eng.* 35:199–202.

Roberts, D. E., L. T. Hersh, and A. M. Scher. 1979. Influence of cardiac fiber orientation on wavefront voltage, conduction velocity, and tissue resistivity in the dog. *Circ. Res.* 44:701–712.

Roth, B. J. 1991. Action potential propagation in a thick strand of cardiac muscle. *Circ. Res.* 68:162–173.

Roth, B. J. 1992. How the anisotropy of the intracellular and extracellular conductivities influences stimulation of cardiac muscle. *J. Math. Biol.* 30:633–646.

Roth, B. J. 1994. Mechanisms for electrical stimulation of excitable tissue. *Crit. Rev. Biomed. Eng.* 22:253–305.

Roth, B. J., and N. Trayanova. 1993. Electrical stimulation in a time-dependent, passive bidomain. *Proc. Ann. Int. Conf. IEEE Eng. Med. Biol. Soc.* 15:857–858.

Roth, B. J., and J. P. Wikswo, Jr. 1994. Electrical stimulation of cardiac tissue: a bidomain model with active membrane properties. *IEEE Trans. Biomed. Eng.* 41:232–240.

Roth, B. J., and J. P. Wikswo, Jr. 1996. The effect of externally applied electrical fields on myocardial tissue. *Proc. IEEE.* 84:379–391.

Rubinstein, J. T. 1991. Analytical theory for extracellular electrical stimulation of nerve with focal electrodes. II. Passive myelinated axon. *Biophys. J.* 60:538–555.

Rubinstein, J. T., and F. A. Spelman. 1988. Analytical theory for extracellular electrical stimulation of nerve with focal electrodes. I. Passive unmyelinated axon. *Biophys. J.* 54:975–981.

Schmidt, J. A., and C. R. Johnson. 1995. DefibSim: an interactive defibrillation device design tool. *Proc. Ann. Int. Conf. IEEE Eng. Med. Biol. Soc.* 17:241–242.

Sepulveda, N. G., B. J. Roth, and J. P. Wikswo, Jr. 1989. Current injection into a two-dimensional anisotropic bidomain. *Biophys. J.* 55:987–999.

Tang, A. S., P. D. Wolf, Y. Afework, W. M. Smith, and R. E. Ideker. 1992. Three-dimensional potential gradient fields generated by intracardiac catheter and cutaneous patch electrodes. *Circulation.* 85:1857–1864.

Trayanova, N. 1996. Discrete versus syncytial tissue behavior in a model of cardiac stimulation. II. Results of simulation. *IEEE Trans. Biomed. Eng.* 43:1141–1150.

Trayanova, N., and T. C. Pilkington. 1993. A bidomain model with periodic intracellular junctions: a one-dimensional analysis. *IEEE Trans. Biomed. Eng.* 40:424–433.

Trayanova, N. A., and B. J. Roth. 1992. Cardiac tissue in an electric field: a study in electrical stimulation. *In* Computers in Cardiology. IEEE Press, Washington, DC. 695–698.

Trayanova, N., and B. J. Roth. 1993. Mechanisms for cardiac stimulation. *Proc. Ann. Int. Conf. IEEE Eng. Med. Biol. Soc.* 15:817–818.

Trayanova, N. A., B. J. Roth, and L. J. Malden. 1993. The response of a spherical heart to a uniform electric field: a bidomain analysis of cardiac stimulation. *IEEE Trans. Biomed. Eng.* 40:899–908.

Walcott, G. P., K. T. Walcott, S. B. Knisley, X. Zhou, and R. E. Ideker. 1994. Mechanisms of defibrillation for monophasic and biphasic waveforms. *Pacing Clin. Electrophysiol.* 17:478–498.

Warman, E. N., W. M. Grill, and D. M. Durand. 1992. Modeling the effects of electric fields on nerve fibers: determination of excitation thresholds. *IEEE Trans. Biomed. Eng.* 39:1244–1254.

Wharton, J. M., P. D. Wolf, W. M. Smith, P.-S. Chen, D. W. Frazier, S. Yabe, N. Danieley, and R. E. Ideker. 1992. Cardiac potential and potential gradient fields generated by single, combined, and sequential shocks during ventricular defibrillation. *Circulation.* 85:1510–1523.

Wikswo, J. P., Jr., S.-F. Lin, and R. A. Abbas. 1995. Virtual electrodes in cardiac tissue: a common mechanism for anodal and cathodal stimulation. *Biophys. J.* 69:2195–2210.

Wikswo, J. P., Jr., T. A. Wisialowski, W. A. Altemeier, J. R. Balser, H. A. Kopelman, and D. M. Roden. 1991. Virtual cathode effects during stimulation of cardiac muscle. Two-dimensional in vivo experiments. *Circ. Res.* 68:513–530.

Witkowski, F. X., and R. E. Kerber. 1991. Currently known mechanisms underlying direct current external and internal cardiac defibrillation. *J. Cardiovasc. Electrophysiol.* 2:562–572.